ELSEVIER

Engineering Analysis with Boundary Elements 29 (2005) 77–91

ENGINEERING ANALYSIS *with* BOUNDARY ELEMENTS

www.elsevier.com/locate/enganabound

Boundary integral equation for inclusion and cavity shape sensitivity in harmonic elastodynamics

Guillermo Rus, Rafael Gallego*

Department of Structural Mechanics, University of Granada, Ed. Politécnico, Avda Fuentenueva s/n, 18002 Granada, Spain

Available online 19 November 2004

Abstract

In many inverse and optimization problems, the computation of the gradient of the response—displacements and tractions—at the boundary of specimens due to a variation of the geometry is needed. Since finite difference techniques are error prone due to the difference parameter and are computationally expensive, a formulation to compute this gradient by direct differentiation is developed based on the boundary integral equation used for the standard Boundary Element Method.

The formulation is implemented and tested for the case of arbitrarily shaped cavities and inclusions in a bounded or unbounded solid in the case of harmonic elastodynamics in 2D. The formulation is developed and studied independently of the discretization and of the parametrization of the change of geometry. The gradient is compared to some simple analytically solvable problems as well as complicated ones solved by centered finite differences for the sake of comparison. All of the cases give very stable and accurate results, both in static and dynamic elasticity.

Keywords: Sensitivity BIE; Direct differentiation; BEM; Inverse problems; Parametrization; Harmonic elastodynamics; Inclusion and cavity detection

1. Introduction

A direct problem can be stated as the calculation of the response (certain field v) given the geometry of the domain (Ω with boundary Γ), mechanical properties (k), physical model (operator L), sources (b), and boundary conditions (some known values of v or its dual variable, say q). In opposition to this, an inverse problem is one in which part of the information above is unknown. If a generic direct problem is defined as,

$$L(k)v + b = 0 \quad \text{on} \quad \Omega \tag{1}$$

different inverse problems can be stated depending on the nature of the unknown (see [11]). To find the missing information, additional data about the response has to be provided, besides the boundary conditions. This additional data v^{ex} is obtained experimentally at some points of the domain or its boundary Γ.

This paper is aimed at the solution of the so called *identification inverse problem* (IIP), where the unknown is the shape of the domain. This problem arises in many branches of science and engineering, but the interest of the authors is mainly the development of computerized non-destructive techniques, aimed at the detection of flaws inside a unreachable part of a mechanical or structural element.

A general inverse problem can be written alternatively as,

(1) the solution of a set of implicit nonlinear equations called observation equations, that relate some properly chosen *design variables* z and the experimental data, v^{ex},

$$F(z) = v^{\text{ex}}$$

(2) or as an optimization problem, where the residual of the former set of equations is minimized,

$$\min_z \frac{1}{2} \|F(z) - v^{\text{ex}}\|^2$$

* Corresponding author.
E-mail addresses: grus@ugr.es (G. Rus), gallego@ugr.es (R. Gallego).

0955-7997/$ - see front matter © 2004 Elsevier Ltd. All rights reserved.
doi:10.1016/j.enganabound.2004.09.001

In both cases, the most effective solution algorithms use sensitivity information (gradient), which should be computed accurately and efficiently.

To perform this computation, besides the obvious but time-consuming finite differences approach, two analytical tools are available: Direct Differentiation Method and Adjoint State Approach. The first one was used by Nishimura [15], Meric [14], Aithal and Saigal [1], Mellings and Aliabadi [13], Lee and Kwak [12], Rus and Gallego [16] and is based on the direct differentiation of the equations, with respect to the geometrical parameters which define the unknown flaw.

On the other hand Bonnet et al., in a series of papers [3–5], applied to the Boundary Integral Equations in elasticity and elastodynamics the Adjoint State Approach. The same approach was used by Burczynski [7] and compared to the direct differentiation.

In this paper a *sensitivity boundary integral equation* or *variation boundary integral equation* is developed, to obtain the sensitivity of displacement and tractions in a harmonic elastodynamics state due to *changes in the geometry of an internal cavity or inclusion*. The equation is obtained by series expansion and linearization, following a procedure first proposed by Tanaka et al. [18] for potential problems, and Saigal et al. [1] for static elasticity. In these papers some terms where missing and a first complete formulation was presented for potential problems by Gallego et al. in 1998 [9]. The final equation should be equivalent to that obtained by Bonnet et al. [4] using material differentiation, but no attempt has been made yet to demonstrate this point.

The obtained equations are thoroughly tested numerically to demonstrate the accuracy of the procedure for the shape gradient computation.

2. Boundary integral equations

In a domain Ω bounded by Γ, the displacement integral equation (or *u*BIE, see [6]) can be written as,

$$c_k^i(\mathbf{y})u_k(\mathbf{y}) + \int_\Gamma [q_k^i(\mathbf{x};\mathbf{y})u_k(\mathbf{x}) - u_k^i(\mathbf{x};\mathbf{y})q_k(\mathbf{x})]\mathrm{d}\Gamma(\mathbf{x}) = 0 \qquad (2)$$

where,

- $u_k(\mathbf{x})$ k-th component of the displacement vector in the actual state at the *observation point* $\mathbf{x}$.
- $q_k(\mathbf{x})$ $\sigma_{jk}(\mathbf{x})n_j(\mathbf{x})$ traction in the actual state at point $\mathbf{x}$. $\sigma_{jk}(\mathbf{x})$ is the stress tensor and n_j the outward normal.
- $u_k^i(\mathbf{x};\mathbf{y})$ k-th component of the displacement vector at the observation point $\mathbf{x}$ due to a point load applied in direction i at the *collocation point* $\mathbf{y}$ (fundamental solution).
- $q_k^i(\mathbf{x};\mathbf{y})$ $=\sigma_{lk}^i(\mathbf{x};\mathbf{y})n_l(\mathbf{x})$ traction of the fundamental solution.
- c_k^i free term whose value depends on the position of the collocation point. Thus, $c_k^i(\mathbf{y}) = \delta_k^i$ (Kroenecker delta) if $\mathbf{y}\in\Omega$ $c_k^i(\mathbf{y})$ depends on the geometry of the boundary at $\mathbf{y}$ if $\mathbf{y}\in\Gamma$, and is such that $c_k^i(\mathbf{y}) = 1/2\delta_k^i$ when the boundary is smooth (continuous normal) at $\mathbf{y}$; $c_k^i(\mathbf{y}) = 0$ otherwise.

The fundamental solution for two-dimensional harmonic elastodynamics is given by

$$u_k^i = \frac{1}{2\pi\mu}[\psi\delta_{ik} - \chi r_{,i}r_{,k}] \qquad (3)$$

$$q_k^i = \frac{1}{2\pi}\left[\left(\phi' - \frac{1}{r}\chi\right)\left(\delta_{ik}r_{,j}n_j + r_{,i}r_{,k}\right) - \frac{2}{r}\chi(n_k r_{,i} - 2r_{,k}r_{,i}r_{,j}n_j\right) - 2\chi' r_{,i}r_{,k}r_{,j}n_j + \left(\frac{c_\mathrm{p}^2}{c_\mathrm{s}^2} - 2\right)\left(\phi' - \chi' - \frac{\chi}{r}\right)r_{,i}n_k\Bigg] \qquad (4)$$

where $r_i = x_i - y_i, r = |\mathbf{r}|$; $r_{,i} = \frac{\partial r}{\partial x_i}$. ψ and χ are functions of the position r and excitation frequency ω, given by the expressions,

$$\psi = \mathrm{K}_0(k_\mathrm{s}r) + \frac{1}{k_\mathrm{s}r}\left[K_1(k_\mathrm{s}r) - \frac{c_\mathrm{s}}{c_\mathrm{p}}\mathrm{K}_1(k_\mathrm{p}r)\right] \qquad (5)$$

$$\chi = \mathrm{K}_2(k_\mathrm{s}r) - \frac{c_\mathrm{s}^2}{c_\mathrm{p}^2}\mathrm{K}_2(k_\mathrm{p}r) \qquad (6)$$

where, $k_\alpha = \frac{i\omega}{c_\alpha}$, and c_p and c_s are the P-waves and S-waves propagation speeds, respectively; $K_n(z)$ is the modified Bessel function of order n.

3. Procedure description

The goal is to calculate the variation of the former integral equation with respect to changes in the geometry of the boundary Γ. The geometrical change is described as an infinitesimal field $\delta x(\mathbf{x})$, such that the coordinates of a point $\mathbf{x}$ change after the perturbation to $\tilde{x}_i = x_i + \delta x_i(\mathbf{x})$. Note that $\mathbf{x}$ is a generic point on the boundary or/and *inside* Ω. This fact, among others, was overlooked in the cited previous works [1,18].

The development of this sensitivity integral equation follows these steps (see illustration in Fig. 1)

(1) The displacement integral equation is established both for the actual domain, and for the perturbed one, with the collocation point at the interior of the domain (i.e. $\mathbf{y}\in\Omega$ but $\mathbf{y}\notin\Gamma$).
(2) A series expansion of the variables in the last one in terms of the infinitesimal perturbation is performed.
(3) Terms higher than linear are neglected and the integral for the actual domain is subtracted.
(4) The ensuing integral equation is taken to the boundary by a careful limiting process as in the standard boundary integral method.

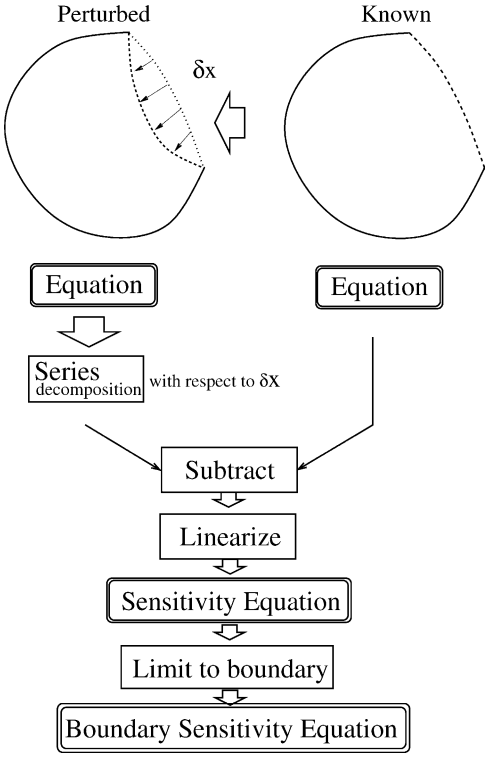

Fig. 1. Procedure for the sensitivity integral equation.

The solution of the ensuing *sensitivity boundary integral equation* (or δ*u*BIE) provides the values of the sensitivities of displacements δ**u** and tractions δ**q** on the boundary with respect to a change of the geometry δ**x**. The sensitivity of a generic cost or objective functional $\mathcal{J}$ defined as,

$$\mathcal{J}(\Gamma_c)=\int_{\Gamma_q}\varphi_u(\mathbf{u})\mathrm{d}\Gamma+\int_{\Gamma_u}\varphi_q(\mathbf{q})\mathrm{d}\Gamma+\int_{\Gamma_f}\psi(\mathbf{x})\mathrm{d}\Gamma \tag{7}$$

could be computed simply applying the chain rule,

$$\delta\mathcal{J}(\Gamma_c)=\int_{\Gamma_q}\frac{\partial\varphi_u}{\partial\mathbf{u}}\delta\mathbf{u}\mathrm{d}\Gamma+\int_{\Gamma_u}\frac{\partial\varphi_q}{\partial\mathbf{q}}\delta\mathbf{q}\mathrm{d}\Gamma+\int_{\Gamma_f}\frac{\partial\psi}{\partial\mathbf{x}}\delta\mathbf{x}\mathrm{d}\Gamma \tag{8}$$

assuming that the fractions of the boundary Γ_q, Γ_u and Γ_f are accessible, and hence fixed.

4. Geometrical sensitivity of the boundary differential and the normal vector

Before developing the complete δ*u*BIE, it is useful to consider the sensitivity of some geometrical quantities that arise in the following sections. To do that, the perturbed domain and any magnitude computed in it, is notated with an upper tilde. The variation of the normal and the boundary differential are defined by the equations,

$$\tilde{\mathbf{n}}=\mathbf{n}+\delta\mathbf{n}+\text{h.o.t.} \tag{9}$$

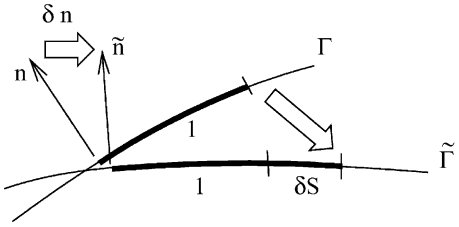

Fig. 2. Variation of the boundary differential.

$$\mathrm{d}\tilde{\Gamma}=(1+\delta S)\mathrm{d}\Gamma+\text{h.o.t.} \tag{10}$$

where h.o.t. stands for *higher order terms*.

4.1. Variation of the boundary differential

In Fig. 2 the relationship between the boundary differential at the actual and perturbed domain are shown. At a boundary point (ξ the boundary differential is defined by,

$$\mathrm{d}\Gamma^2=\mathrm{d}\xi_i\mathrm{d}\xi_i \tag{11}$$

After the perturbation $\boldsymbol{\xi}=\xi+\delta\xi$, and therefore the differential fulfills the equation,

$$\mathrm{d}\tilde{\Gamma}^2=(\mathrm{d}\xi_i+\mathrm{d}\delta\xi_i)(\mathrm{d}\xi_i+\mathrm{d}\delta\xi_i) \tag{12}$$

Expanding the product and neglecting terms higher than linear,

$$\mathrm{d}\tilde{\Gamma}^2\simeq\mathrm{d}\Gamma^2+2\mathrm{d}\xi_i\mathrm{d}\delta\xi_i=2\mathrm{d}\xi_i\delta\xi_{i,j}\mathrm{d}\xi_j \tag{13}$$

Taking the square root and neglecting again higher order terms,

$$\mathrm{d}\tilde{\Gamma}\simeq\mathrm{d}\Gamma(1+\delta\xi_{i,j}t_it_j) \tag{14}$$

where

$$t_i=\frac{\mathrm{d}\xi_i}{\mathrm{d}\Gamma} \tag{15}$$

are the components of the tangent vector at ξ. Therefore, recovering Eq. (10),

$$\delta S=\delta\xi_{i,j}t_it_j \tag{16}$$

4.2. Variation of the normal vector

In Fig. 3 the variation of the normal at a boundary point is represented. To obtain the variation of the normal vector, it is more convenient to compute first the variation of the tangent vector. Their components after the perturbation are,

$$\tilde{t}_i=\frac{\mathrm{d}\tilde{\xi}_i}{\mathrm{d}\tilde{\Gamma}}=\frac{\mathrm{d}\xi_i+\mathrm{d}\delta\xi_i}{\mathrm{d}\Gamma(1+\delta S)} \tag{17}$$

Expanding Eq. (17) and neglecting terms higher than linear,

$$\tilde{t}_i\simeq t_i-t_i\delta S+\delta\xi_{i,j}t_j \tag{18}$$

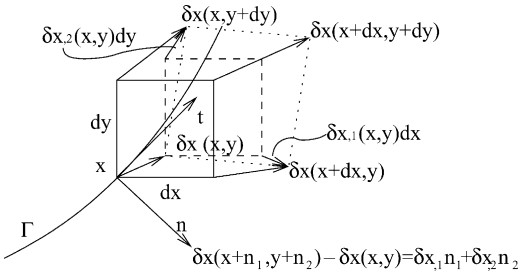

Fig. 3. Differential geometrical in the vicinity of ξ.

Since only the non-parallel component affects the variation of the normal, the second term is dropped out,

$$\tilde{t}_i \simeq t_i + \delta\xi_{i,j}t_j \tag{19}$$

Now, the normal is perpendicular to the tangent vector,

$$\tilde{n}_i \simeq n_i + \varepsilon_{ik}\delta\xi_{k,j}t_j \tag{20}$$

where ε_{ik} is the permutation tensor. To maintain the unit modulus, only the component of the variation perpendicular to the normal is kept,

$$\tilde{n}_i \simeq n_i + t_i t_l \varepsilon_{lk}\delta\xi_{k,j}t_j \tag{21}$$

Therefore,

$$\delta\mathbf{n} \simeq -n_j\delta\xi_{j,k}t_k\mathbf{t} \tag{22}$$

5. Variation of the integral equation

Consider Eq. (2) for a domain point $\mathbf{y}$, i.e. one *within* the body Ω.

$$u_i(\mathbf{y}) + \int_\Gamma [q_k^i(\mathbf{x};\mathbf{y})u_k(\mathbf{x}) - u_k^i(\mathbf{x};\mathbf{y})q_k(\mathbf{x})]\mathrm{d}\Gamma(\mathbf{x}) = 0 \tag{23}$$

The displacements and tractions change to $\tilde{u}_i(\tilde{\mathbf{x}})$ and $\tilde{q}_i(\tilde{\mathbf{x}})$ when the geometry is perturbed to $\tilde{\Omega}$. We now define the *variation* or *sensitivities of displacements* and *tractions* δu_i and δq_i in,

$$\tilde{u}_i(\tilde{\mathbf{x}}) = u_i(\mathbf{x}) + \delta u_i(\mathbf{x}) \tag{24}$$

$$\tilde{q}_i(\tilde{\mathbf{x}}) = q_i(\mathbf{x}) + \delta q_i(\mathbf{x}) \tag{25}$$

Note that these variations are *material*, meaning that they include the change due to the modification of the geometry (Ω to $\tilde{\Omega}$), as well as those due to the change in the point of computation ($\mathbf{x}$ to $\tilde{\mathbf{x}}$). To find the equations that these variations fulfill, the integral equation is written for the perturbed domain,

$$\tilde{u}_i(\tilde{\mathbf{y}}) + \int_{\tilde{\Gamma}} [q_k^i(\tilde{\mathbf{x}};\tilde{\mathbf{y}})\tilde{u}_k(\tilde{\mathbf{x}}) - u_k^i(\tilde{\mathbf{x}};\tilde{\mathbf{y}})\tilde{q}_k(\tilde{\mathbf{x}})]\mathrm{d}\tilde{\Gamma}(\tilde{\mathbf{x}}) = 0 \tag{26}$$

The kernels in this equation are computed at perturbed points. It is simple to relate them to the kernels at the actual points by Taylor series expansion,

$$u_k^i(\tilde{\mathbf{x}};\tilde{\mathbf{y}}) = u_k^i(\mathbf{x};\mathbf{y}) + \frac{\partial u_k^i}{\partial x_m}\delta x_m + \frac{\partial u_k^i}{\partial y_m}\delta y_m + \text{h.o.t.} \tag{27}$$

Taking into account that the kernels are radial functions of $r_i = x_i - y_i$, then

$$u_k^i(\tilde{\mathbf{x}};\tilde{\mathbf{y}}) = u_k^i(\mathbf{x};\mathbf{y}) + \frac{\partial u_k^i}{\partial r_m}\delta x_m - \frac{\partial u_k^i}{\partial r_m}\delta y_m + \text{h.o.t.} \tag{28}$$

or more compactly,

$$u_k^i(\tilde{\mathbf{x}};\tilde{\mathbf{y}}) = u_k^i(\mathbf{x};\mathbf{y}) + u_{k,m}^i\delta r_m + \text{h.o.t.} \tag{29}$$

where the comma stands for derivation with respect to the coordinates of the observation point $\mathbf{x}$.

For the kernel $q_k^i(\tilde{\mathbf{x}};\tilde{\mathbf{y}})$ the variation of the normal has to be taken into account since,

$$q_k^i(\tilde{\mathbf{x}};\tilde{\mathbf{y}}) = \tilde{\sigma}_i^{jk}(\tilde{\mathbf{x}};\tilde{\mathbf{y}})\tilde{n}_j(\tilde{\mathbf{x}}) \tag{30}$$

First, by Taylor expansion,

$$\sigma_{jk}^i(\tilde{\mathbf{x}};\tilde{\mathbf{y}}) = \sigma_{jk}^i(\mathbf{x};\mathbf{y}) + \sigma_{jk,m}^i(\mathbf{x};\mathbf{y})\delta r_m + \text{h.o.t.} \tag{31}$$

and plugging in Eq. (30) this expansion and that of the normal (Eq. (22)),

$$q_k^i(\tilde{\mathbf{x}};\tilde{\mathbf{y}}) = q_k^i(\mathbf{x};\mathbf{y}) + \sigma_{jk}^i(\mathbf{x};\mathbf{y})\delta n_j(\mathbf{x}) + \sigma_{jk,m}^i(\mathbf{x};\mathbf{y})\delta r_m n_j(\mathbf{x}) + \text{h.o.t.} \tag{32}$$

Finally, the integral along the perturbed domain can be transformed to the actual domain by,

$$\int_{\tilde{\Gamma}}(\ldots)\mathrm{d}\tilde{\Gamma} = \int_\Gamma(\ldots)(1+\delta S)\mathrm{d}\Gamma + \text{h.o.t.} \tag{33}$$

Collecting all the expressions above, substituting them in the integral Eq. (26), subtracting Eq. (23), and neglecting terms higher than linear, the following integral equation is obtained,

$$\begin{aligned}\delta u_i(\mathbf{y}) &+ \int_\Gamma [q_k^i(\mathbf{x};\mathbf{y})\delta u_k(\mathbf{x}) - u_k^i(\mathbf{x};\mathbf{y})\delta q_k(\mathbf{x})]\mathrm{d}\Gamma(\mathbf{x}) \\ &= \int_\Gamma \{[u_{k,m}^i(\mathbf{x};\mathbf{y})q_k(\mathbf{x}) - \sigma_{jk,m}^i(\mathbf{x};\mathbf{y})n_j(\mathbf{x})u_k(\mathbf{x})]\delta r_m \\ &\quad + [u_k^i(\mathbf{x};\mathbf{y})q_k(\mathbf{x}) - q_k^i(\mathbf{x};\mathbf{y})u_k(\mathbf{x})]\delta S(\mathbf{x}) \\ &\quad - \sigma_{jk}^i(\mathbf{x};\mathbf{y})u_k(\mathbf{x})\delta n_j(\mathbf{x})\}\mathrm{d}\Gamma(\mathbf{x})\end{aligned} \tag{34}$$

This integral equation relates the displacement variation at a domain point $\mathbf{y}$ with the variation of displacements and tractions at the boundary points, and the variation of the geometry of the boundary.

Note, firstly, that the kernels on the left hand side integral are those of the original integral Eq. (2). Secondly, in the integrand in the right hand side appear the same kernels, their first derivatives, the displacement and tractions on

the boundary at the actual configuration, and the variation of the geometry and its derivatives.

6. Limit to the boundary

The integral equation obtained in the previous section would be useful to compute sensitivities at interior points, but its *boundary* counterpart provides the relationship between the sensitivities of displacements and tractions along the boundary *only* and the variation of the geometry.

In order to perform the limit, a point $\mathbf{y}$ at the boundary is considered, and the actual boundary is distorted as shown in Fig. 4

Carrying out the usual decomposition of the boundary integral,

$$\int_{\Gamma}(\ldots)\mathrm{d}\Gamma \rightarrow \int_{\Gamma-\Gamma_\varepsilon}(\ldots)\mathrm{d}\Gamma + \int_{S_\varepsilon}(\ldots)\mathrm{d}\Gamma \tag{35}$$

the limit to the boundary of each term in Eq. (34) can be computed. The first integral converges in all cases, while the second tends to zero or yields a free term.

For the left hand side terms in Eq. (34),

$$\lim_{\varepsilon\to 0}\left\{\delta u_i(\mathbf{y}) + \int_{\Gamma}[q_k^i\delta u_k - u_k^i\delta q_k]\mathrm{d}\Gamma\right\}$$

$$= c_k^i\delta u_k(\mathbf{y}) + \int_{\Gamma}[q_k^i\delta u_k - u_k^i\delta q_k]\mathrm{d}\Gamma \tag{36}$$

where c_k^i is the usual free term, since the kernels in this integral are those of the standard integral equation. The integrals in the right hand side of this expression are understood as improper or Cauchy Principal Value. For this limit to exist, the following expansion should hold,

$$\delta u_k(\mathbf{x}) = \delta u_k(\mathbf{y}) + \text{h.o.t.} \tag{37}$$

i.e. δu_k has to be continuous at $\mathbf{y}$. In addition $\delta q_k(\mathbf{x})$ has to be bounded.

For the computation of the remaining integrals along the circular path S_ε, the order of the kernels has first to be assessed. This analysis leads to,

$$u_k^i(\mathbf{x};\mathbf{y}) = O(\ln r)\ \sigma_{jk}^i = O\left(\frac{1}{r}\right)$$

$$u_{k,m}^i(\mathbf{x};\mathbf{y}) = O\left(\frac{1}{r}\right)\ \sigma_{jk,m}^i = O\left(\frac{1}{r^2}\right)$$

To yield a finite integrand the rest of the variables in the integrands have to be expanded to the proper order. For instance,

$$\lim_{\varepsilon\to 0}\int_{S_\varepsilon} u_{k,m}^i(\mathbf{x};\mathbf{y})q_k(\mathbf{x})\delta r_m\mathrm{d}S_\varepsilon$$

$$= \sigma_{jk}(\mathbf{y})\delta y_{m,l}\lim_{\varepsilon\to 0}\varepsilon^2\int_{\theta_1}^{\theta_2} u_{k,m}^i n_j n_l\mathrm{d}\theta = 0 \tag{38}$$

because the order of the integrand is only $O(1/\varepsilon)$. To arrive at this result, the expansions,

$$q_k(\mathbf{x}) = n_j(\mathbf{x})\sigma_{jk}(\mathbf{y}) + \text{h.o.t.} \tag{39}$$

$$\delta r_m = \delta y_{m,l}(x_l - y_l) + \text{h.o.t.} \tag{40}$$

should exist. The facts that $\mathrm{d}S_\varepsilon = \varepsilon\ \mathrm{d}\theta$ and $x_l - y_l = \varepsilon n_l$ on the circular boundary have been considered. In the same manner,

$$\lim_{\varepsilon\to 0}\int_{S_\varepsilon}\sigma_{jk,m}^i(\mathbf{x};\mathbf{y})n_j(\mathbf{x})u_k(\mathbf{x})\delta r_m\mathrm{d}S_\varepsilon$$

$$= u_k(\mathbf{y})\delta y_{m,l}\lim_{\varepsilon\to 0}\varepsilon^2\int_{\theta_1}^{\theta_2}\sigma_{jk,m}^i n_j n_l\mathrm{d}\theta = t_{kml}^{1i}u_k(\mathbf{y})\delta y_{m,l} \tag{41}$$

$$\lim_{\varepsilon\to 0}\int_{S_\varepsilon} u_k^i(\mathbf{x};\mathbf{y})q_k(\mathbf{x})\delta S(\mathbf{x})\mathrm{d}S_\varepsilon$$

$$= \sigma_{jk}(\mathbf{y})\delta S(\mathbf{y})\lim_{\varepsilon\to 0}\varepsilon\int_{\theta_1}^{\theta_2} u_k^i n_j\mathrm{d}\theta = 0 \tag{42}$$

$$\lim_{\varepsilon\to 0}\int_{S_\varepsilon} q_k^i(\mathbf{x};\mathbf{y})u_k(\mathbf{x})\delta S(\mathbf{x})\mathrm{d}S_\varepsilon$$

$$= u_k(\mathbf{y})\delta y_{m,l}\lim_{\varepsilon\to 0}\varepsilon\int_{\theta_1}^{\theta_2} q_k^i t_l t_m\mathrm{d}\theta = t_{kml}^{2i}u_k(\mathbf{y})\delta y_{m,l} \tag{43}$$

$$\lim_{\varepsilon\to 0}\int_{S_\varepsilon}\sigma_{jk}^i(\mathbf{x};\mathbf{y})u_k(\mathbf{x})\delta n_j(\mathbf{x})\mathrm{d}S_\varepsilon$$

$$= u_k(\mathbf{y})\delta y_{m,l}\lim_{\varepsilon\to 0}\varepsilon\int_{\theta_1}^{\theta_2}\sigma_{jk}^i\varepsilon_{hm}t_j t_h t_l\mathrm{d}\theta = t_{kml}^{3i}u_k(\mathbf{y})\delta y_{m,l} \tag{44}$$

To arrive at these expressions the following expansions were considered,

$$u_k(\mathbf{x}) = u_k(\mathbf{y}) + \text{h.o.t.} \tag{45}$$

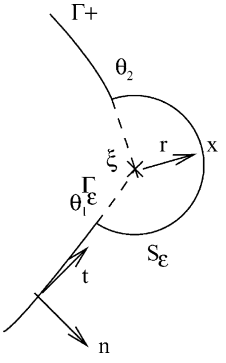

Fig. 4. Circular distortion around boundary point.

$$\delta x_m = \delta y_m + \delta y_{m,j}(x_j - y_j) + \text{h.o.t.} \tag{46}$$

Besides, $q_k(\mathbf{x})$ has to be bounded.

Collecting terms, the *Sensitivity Boundary Integral Equation* for the displacements (or δuBIE) is finally,

$$\begin{aligned} & c^i_k(\mathbf{y})\delta u_k(\mathbf{y}) + t^i_{klm}(\mathbf{y})u_k(\mathbf{y})\delta y_{l,m} + \int_\Gamma [q^i_k(\mathbf{x};\mathbf{y})\delta u_k(\mathbf{x}) \\ & - u^i_k(\mathbf{x};\mathbf{y})\delta q_k(\mathbf{x})]\mathrm{d}\Gamma(\mathbf{x}) \\ & = \int_\Gamma \{[u^i_{k,m}(\mathbf{x};\mathbf{y})q_k(\mathbf{x}) - \sigma^i_{jk,m}(\mathbf{x};\mathbf{y})n_j(\mathbf{x})u_k(\mathbf{x})]\delta r_m \\ & + [u^i_k(\mathbf{x};\mathbf{y})q_k(\mathbf{x}) - q^i_k(\mathbf{x};\mathbf{y})u_k(\mathbf{x})]\delta S(\mathbf{x}) \\ & - \sigma^i_{jk}(\mathbf{x};\mathbf{y})u_k(\mathbf{x})\delta n_j(\mathbf{x})\}\mathrm{d}\Gamma(\mathbf{x}) \end{aligned} \tag{47}$$

where $t^i_{klm}(\mathbf{y})$ is a free term that can be evaluated from Eqs. (41), (43), and (44). The integrals are understood in the CPV sense. This equation is valid for *any point* on the boundary *smooth or not* and relates the variations of displacement and tractions on the boundary to the variation of the geometry.

The second free term appears to have been overlooked in the literature. At a smooth boundary point this free term vanishes and the equation simplifies to,

$$\begin{aligned} & \frac{1}{2}\delta u_i(\mathbf{y}) + \int_\Gamma [q^i_k(\mathbf{x};\mathbf{y})\delta u_k(\mathbf{x}) - u^i_k(\mathbf{x};\mathbf{y})\delta q_k(\mathbf{x})]\mathrm{d}\Gamma(\mathbf{x}) \\ & = \int_\Gamma \{[u^i_{k,m}(\mathbf{x};\mathbf{y})q_k(\mathbf{x}) - \sigma^i_{jk,m}(\mathbf{x};\mathbf{y})n_j(\mathbf{x})u_k(\mathbf{x})]\delta r_m \\ & + [u^i_k(\mathbf{x};\mathbf{y})q_k(\mathbf{x}) - q^i_k(\mathbf{x};\mathbf{y})u_k(\mathbf{x})]\delta S(\mathbf{x}) \\ & - \sigma^i_{jk}(\mathbf{x};\mathbf{y})u_k(\mathbf{x})\delta n_j(\mathbf{x})\}\mathrm{d}\Gamma(\mathbf{x}) \end{aligned} \tag{48}$$

6.1. Remarks about the continuity requirements for boundary variables

For arriving to the δuBIE the boundary variables should fulfill certain conditions demanded by the expansions to the required order. In Table 1 the continuity requirements are summarized.

Table 1
Continuity requirements for each variable at the collocation point—means no conditions to fulfill and $C^{1,\alpha}$ means the Hölder condition, with $0 \le \alpha < 1$

Variable	In uBIE	In δuBIE
u_k	$C^{0,\alpha}$	$C^{0,\alpha}$
q_k	Bounded	Bounded
σ_{kl}	–	$C^{0,\alpha}$
δx_l	–	$C^{1,\alpha}$
δu_l	–	$C^{0,\alpha}$
δq_l	–	$C^{0,\alpha}$
$\delta\sigma_{kl}$	–	–

These conditions have importance in the discretization and collocation method used to solve numerically the equations, since the same conditions should be fulfilled by the interpolated variables exact or approximately, to avoid computational errors.

7. Numerical solution of the sensitivity displacement BIE

Standard boundary element techniques are employed to solve the δuBIE. The boundary is divided into a number of elements, and within each one the geometry, displacements, tractions and their variations are interpolated quadratically, where ϕ_n are standard quadratic base functions,

$$\mathbf{x} = \sum_{n=1}^{3}\phi_n\mathbf{x}^n \quad \mathbf{u} = \sum_{n=1}^{3}\phi_n\mathbf{u}^n \quad \mathbf{q} = \sum_{n=1}^{3}\phi_n\mathbf{q}^n$$

$$\delta\mathbf{u} = \sum_{n=1}^{3}\phi_n\mathbf{u}^n\delta\mathbf{q} = \sum_{n=1}^{3}\phi_n\mathbf{q}^n$$

7.1. Collocation

Using these standard elements, the continuity conditions fulfilled by the approximation are given in Table 2.

These results show that the collocation points for the δuBIE can be placed at the standard locations, although, to simplify the computation, at corners, multiple collocation inside the adjacent elements are performed.

7.2. Parametrization

The variation of the geometry during a step in the iterative inverse solution is represented by a so called parameterization, which stands for a representation of the geometry by a finite set of values. Many inverse problems are ill-posed: solutions may not exist, there may be multiple solutions, or they could be non-continuous with respect to the data. The iterative numerical methods for highly nonlinear and ill-conditioned equations that deal with this kind of problems are never guaranteed to converge, but the 'probability' of convergence highly depend on the number of parameters to search.

Table 2
Continuity fulfillments for each variable at the collocation point. (1) Depends on the parameterization of the variable boundary. C^∞ is fulfilled using a continuous variation field, as shown in Section 7.2

Component	Between elements	Inside elements
u_k	$C^{0,\alpha}$	C^∞
q_k	$C^{0,\alpha}$	C^∞
σ_{kl}	$C^{0,\alpha}$	C^∞
δx_l	(1)	(1)
δu_l	$C^{0,\alpha}$	C^∞
δq_l	$C^{0,\alpha}$	C^∞
$\delta\sigma k_l$	$C^{0,\alpha}$	C^∞

This ill-conditioning is rooted in the physical meaning of the problem, and to solve this a reduced number of unknowns is employed, which amounts to a regularization of the problem.

There is a wide range of alternative parameterizations. The most usual ones are based on a definition of the complete geometry by splines of all kinds and orders. In identification problems, the geometry is usually defined by simple geometrical entities, in turn defined by a few parameters (like ellipses defined by the coordinates of the center, the axes length and an angle of orientation [2,13,19]).

A different approach first put forward by Gallego and Suárez [8] consists in defining directly the variation field instead of the geometry, since it is not needed. The advantage of this approach is that it can be applied to initial geometries of any shape, and it is not limited, therefore, to any set of simple shapes.

The variation field δx_i expresses the change of position of each material point,

$$\tilde{x}_i = x_i + \delta x_i \tag{49}$$

The parametrization is defined as,

$$\delta x_i(\mathbf{x}) = \Theta_{ig}(\mathbf{x})\delta P_g \tag{50}$$

in terms of a finite number of parameters δP_g and a known parametrization matrix $\Theta_{ig}(\mathbf{x})$. The simplest parametrization is described by a constant *virtual deformation field*. This is represented by the following parametrization matrix,

$$(\Theta_{ig}) = \begin{bmatrix} 1\,0 & x_2 - x_2^0 & x_1 - x_1^0 & x_1 - x_1^0 & x_2 - x_2^0 \\ 0\,1 & -(x_1 - x_1^0)\, x_2 - x_2^0 & -(x_2 - x_2^0)\, x_1 - x_1^0 & & \end{bmatrix} \tag{51}$$

where $\mathbf{x}^0$ is an arbitrary point, for instance the centroid of the flaw. The elements of the parameter vector δP_g has the following physical (virtual) meaning,

$$(\delta P_g) = \begin{bmatrix} \delta x_1^0 \\ \delta x_2^0 \\ \delta\omega \\ \delta\varepsilon_m \\ \delta\varepsilon' \\ \delta\varepsilon_{12} \end{bmatrix} = \begin{bmatrix} \text{Variation of first coordinate of the centroid of the flaw} \\ \text{Variation of second coordinate of the centroid of the flaw} \\ \text{Angle of rotation} \\ \text{Spheric strain} \\ \text{Horizontal elongation} \\ \text{Distortion} \end{bmatrix} \tag{52}$$

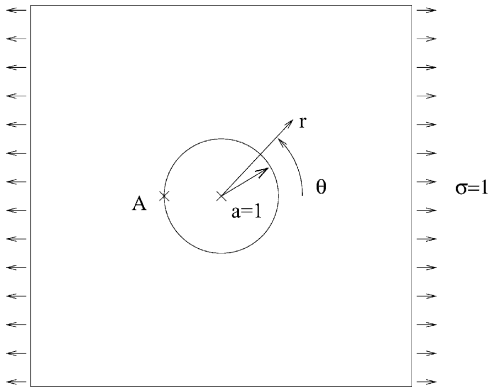

Fig. 5. Circular flaw in an infinite plate subject to remote uniform loading.

With this parametrization the variable boundary changes as if it were subject to a constant deformation field, modifying its shape and location. Regardless of its initial shape (circular, elliptical, squared, etc.) the same parametrization can be used. Note that this representation for $\delta x_i(\mathbf{x})$ is C^∞.

8. Discrete system of equations

Applying the boundary discretization and approximation to the δuBIE and collocating the equation at the nodes, the left hand side of Eq. (47) leads to,

$$\mathbf{H}\delta\mathbf{u} - \mathbf{G}\delta\mathbf{q} \tag{53}$$

where $\mathbf{H}$ and $\mathbf{G}$ are the standard boundary element matrices, while $\delta\mathbf{u}$ and $\delta\mathbf{q}$ collect the variations of displacements and tractions at the boundary nodes.

On the other hand, substituting the linear parametrization on the right hand side of Eq. (47) the following expression is

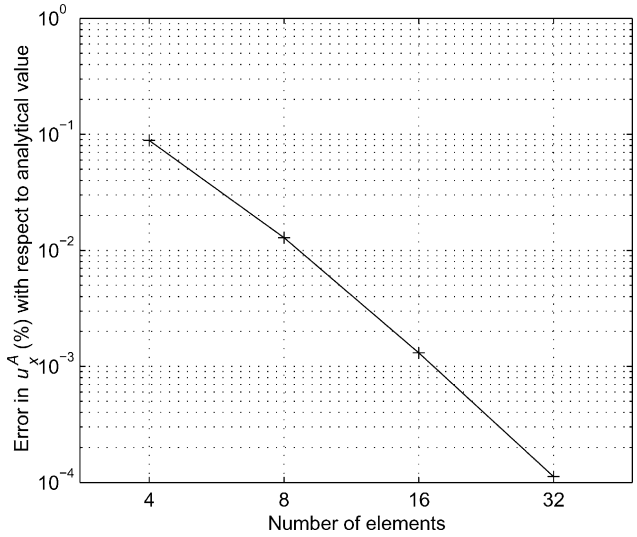

Fig. 6. Convergence of horizontal displacement sensitivity at point A with increasing number of elements (+ analytical solution, − numerical solution).

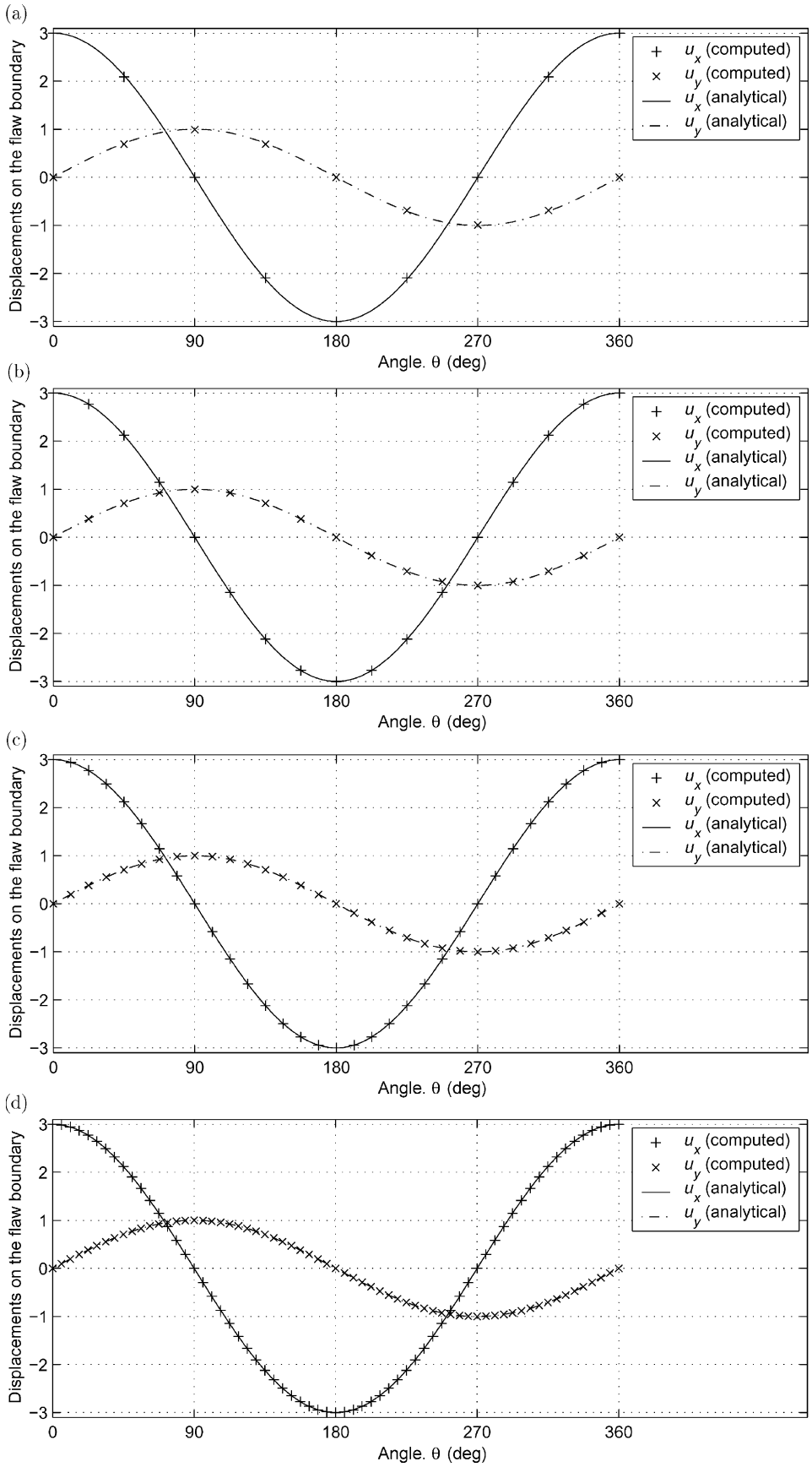

Fig. 7. Displacement sensitivity along the boundary for different meshes: (a) four elements, (b) eight elements, (c) sixteen element, (d) thirty-two elements.

Table 3
Error (%) in displacement sensitivities with respect to analytical solution along the boundary for different meshes (*NaN*: at points where the analytical solution is nil and the relative error cannot be computed)

Point pos. (degrees)	Four elements (%)		Eight elements ($\%\times10^{-2}$)		16 Elements ($\%\times10^{-3}$)		32 Elements ($\%\times10^{-4}$)	
	δu_x	δu_y	δu_x	δu_y	δu_x	δu_y	δu_x	δu_y
0.00000	0.088	NaN	1.287	NaN	1.306	NaN	1.123	NaN
11.2500					4.030	16.66	1.366	15.38
16.8750							2.966	8.153
22.5000			6.626	25.36	2.343	15.46	1.680	7.706
33.7500					5.177	13.15	2.370	6.593
39.3750							3.262	6.135
45.0000	1.365	2.360	6.420	9.515	4.820	8.282	2.658	4.891
56.2500					6.897	8.103	3.365	3.963
61.8750							3.953	4.617
67.5000			12.39	8.086	7.122	0.819	3.173	1.693
78.7500					8.111	4.687	7.162	0.110
84.3750							3.982	2.672
90.0000	3.175	0.932	NaN	5.882	NaN	2.268	NaN	0.061
101.250					8.111	4.687	7.162	0.110
106.875							4.120	4.326
112.500			12.39	8.086	7.122	0.819	3.173	1.693
123.750					6.897	8.103	3.365	3.963
129.375							3.440	5.394
135.000	1.365	2.360	6.420	9.515	4.820	8.282	2.658	4.891
146.250					5.177	13.15	2.370	6.593
151.875							3.259	7.905
157.500			6.626	25.36	2.343	15.46	1.680	7.706
168.750					4.030	16.66	1.366	15.38
174.375							2.635	8.830

obtained,

$$ {}^{g}U_i^g(\xi)\delta P_g \tag{54}$$

where,

$$\begin{aligned} {}^{g}U_i^g(\xi) = \int_\Gamma [&(u^i_{k,m}(\mathbf{x},\xi)q_k - \sigma^i_{jk,m}(\mathbf{x},\xi)n_j(\mathbf{x})u_k(\mathbf{x}))(\Theta_{ig}(\xi) \\ &- \Theta_{ig}(\mathbf{x})) + (u^i_k(\mathbf{x},\xi)q_k \\ &- \sigma^i_{jk}(\mathbf{x},\xi)n_j(\mathbf{x})u_k(\mathbf{x}))t_k t_l \Theta_{lg,k} \\ &- \sigma^i_{jk}(\mathbf{x},\xi)u_k(\mathbf{x})t_i t_m t_l \varepsilon_{mk}\Theta_{kg,l}(\mathbf{x})]\mathrm{d}\Gamma(\mathbf{x}) \end{aligned} \tag{55}$$

Applying the equation at every collocation point, the following system of algebraic equations is obtained,

$$\mathbf{H}\delta\mathbf{u} - \mathbf{G}\delta\mathbf{q} = \Delta\delta\mathbf{P} \tag{56}$$

where $\delta\mathbf{P}$ is the parameter set. Δ is a $2N\times M$ matrix that contains the elements ${}^{g}U_i^h(\xi)$, where N is the number of nodes and M the number of parameters.

When dealing with inclusions, the subregioning approach has been used. The δuBIE s for the matrix and the inclusion are established and the equations are coupled using the equilibrium and compatibility conditions, as in the standard formulation.

8.1. Computation of the shape sensitivities

Eq. (56) can be solved for an arbitrary value of the parameters $\delta\mathbf{P}$. The application of the boundary conditions for displacement and traction variations yield the same system matrix $\mathbf{A}$ as the standard BEM, since the prescribed

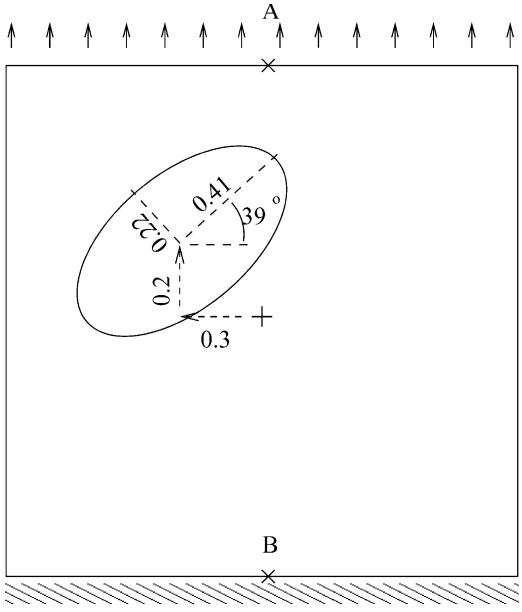

Fig. 8. Flaw location and shape (cavity or inclusion).

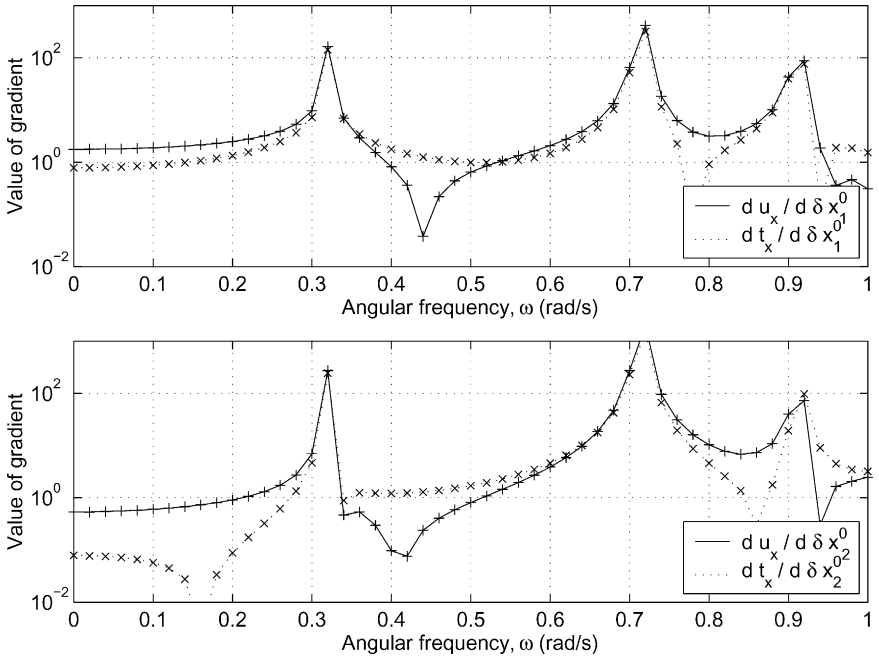

Fig. 9. Modulus of gradient for a variable cavity; continuous lines show the value obtained using δuBIE; dots, finite difference values. Upper graph, sensitivity with respect to δx_1^0, lower graph, sensitivity with respect to δx_2^0.

values have zero variation, yielding,

$$\mathbf{A}\delta\mathbf{v} = \Delta\delta\mathbf{P} \tag{57}$$

where $\delta\mathbf{v}$ groups the variation of displacement and traction at boundary point where they are not prescribed.

The solutions of this system of equations for each column of $\mathbf{\Delta}$ can be performed and grouped into ${}^{g}\mathbf{J}$, which has the meaning of a *shape Jacobian*, so that,

$$\delta\mathbf{v} = {}^{g}\mathbf{J}\delta\mathbf{P} \tag{58}$$

From a computational point of view, this procedure is very cheap since the system matrix $\mathbf{A}$ is already computed and factorized to compute the displacement and traction fields on the boundary, so the computation

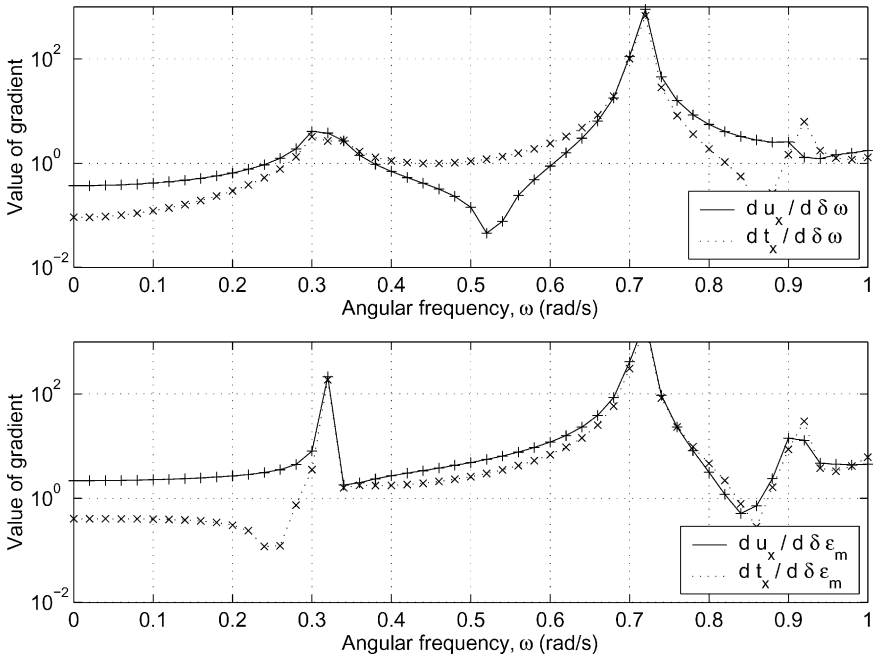

Fig. 10. Modulus of gradient for a variable cavity; continuous lines show the value obtained using δuBIE; dots, finite difference values. Upper graph, sensitivity with respect to $\delta\omega$, lower graph, sensitivity with respect to $\delta\varepsilon_m$.

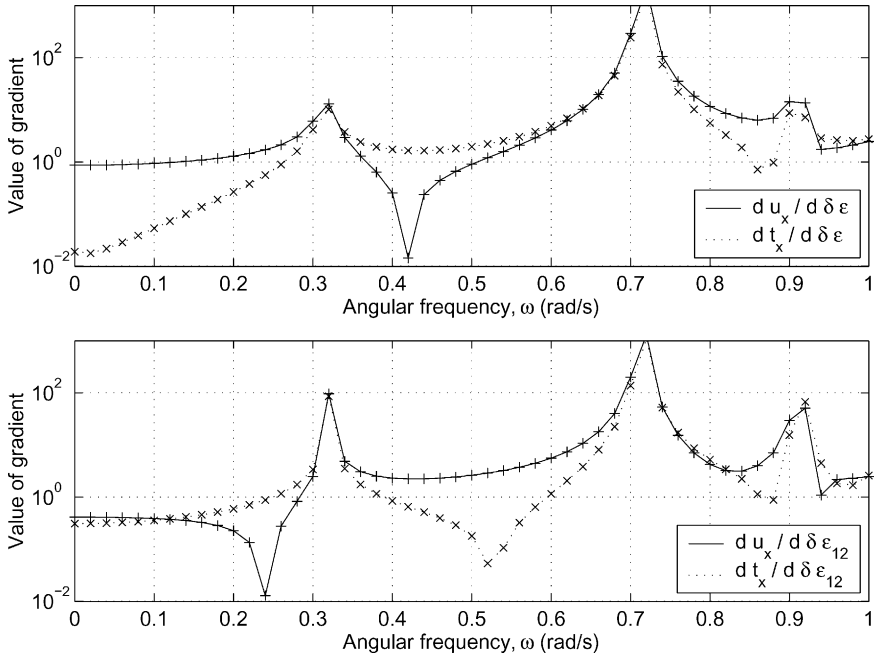

Fig. 11. Modulus of gradient for a variable cavity; continuous lines show the value obtained using δuBIE; dots, finite difference values. Upper graph, sensitivity with respect to $\delta\varepsilon'$, lower graph, sensitivity with respect to $\delta\varepsilon_{12}$.

of the shape jacobian only entails forward and back substitutions for the M columns of matrix $\mathbf{\Delta}$, where M is usually a very low number.

Eq. (58) allows the computation of the linear variation of any boundary displacement or traction for a given virtual deformation of the flaw. The elements of the shape Jacobian represent the derivative or sensitivity of the boundary variables with respect to the shape parameters.

9. Sensitivity tests

In a series of applications the sensitivity is computed and the results are compared to analytical ones, when available or with results obtained by central finite differences.

9.1. Circular cavity in an infinite domain in elastostatics

In the first application a simple elastostatic problem is considered, since its analytical solution is known and the shape sensitivity can be computed by simple differentiation.

Consider a circular cavity in an infinite domain, (see Fig. 5), subject to remote uniform tension. The displacement along the cavity boundary is analytically known [10,17]:

$$u_x = \frac{\sigma cos\theta(a^4(1+\nu) - a^2(-3+\nu)r^2 + 2r^4 - 2a^2(1+\nu)(a^2-r^2)cos2\theta}{2Er^3}\, u_y$$

$$= \frac{-\sigma(a^4(1+\nu) + a^2(1-3\nu)r^2 + 2\nu r^4 + 2a^2(1+\nu)(a^2-r^2)cos2\theta)sin\theta}{2Er^3}$$

where a is the radius of the cavity.

The material derivative with respect to the radius of the cavity particularized at its boundary is given by,

$$u_{x,a} = \frac{3\sigma cos\theta}{E}$$

$$u_{y,a} = \frac{-\sigma sin\theta}{E}$$

The shape sensitivity has been computed using the δuBIE with respect to the parameter $\delta\varepsilon_m$ which is equivalent to the variation of radius. The error of the sensitivity of the horizontal displacement at point A compared to the exact solution is shown in Fig. 6, for discretizations of the cavity of 4, 8, 16 and 32 elements. The collocation strategy is to move the first and last nodes of the elements inwards by 20% throughout.

The following four graphics show the values of the two components of the displacement variation for all the nodes versus the analytical solution in the case of 4, 8, 16 and 16 elements (Fig. 7). In Table 3 the error (%) between the analytical and the computed solution for the different meshes is presented.

Note that even with a very coarse mesh (four quadratic elements), the numerical solution is indistinguishable from the analytical one. The numerical error is about 1% in this case as shown in Table 3 below.

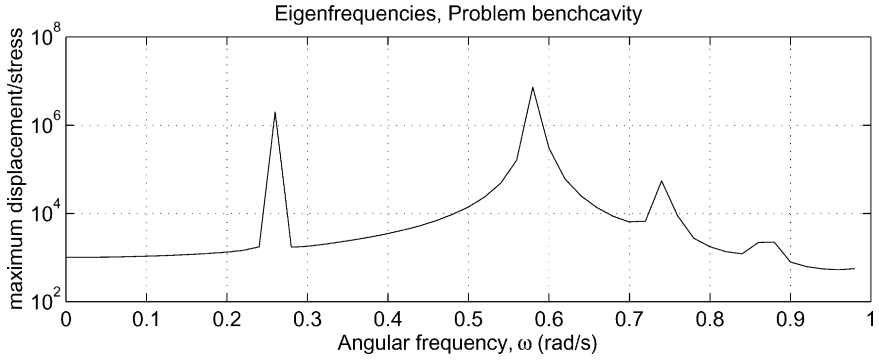

Fig. 12. Plate with a cavity: amplification factor for $u_y(A)$ vs. the excitation frequency.

9.2. Comparison with numerical solutions

Sensitivity tests are performed using two benchmark problems for the sake of reproducibility and simplicity of comparison. The external shape and boundary conditions of the known body are common for both problems, one with a cavity and the other with an inclusion (see Fig. 8).

The fixed contour consists of a 2×2 box of a material with material properties $E=1.0$; $\nu=0.2$, $\rho=1.0$. In the case of an inclusion, it is made of a softer material with $E=0.5$, and the same remaining material constants. As boundary conditions, the lower side is fixed and the upper side is subjected to an uniform unitary vertical stress with varying frequency. Eight quadratic elements are used to discretize each of the outer sides of the boundary and 32 for the flaw boundary, making a total of 64 elements.

The boundary of the cavity or inclusion is defined as an ellipse of center $(-0.3, 0.2)$, semiaxes 0.41 and 0.22, and inclined 39 degrees with respect to the horizontal axis.

Only at two points the values of sensitivities are shown: at point A the sensitivity of horizontal displazament, and at point B the sensitivity of horizontal traction. For the sake of comparison, the sensitivities are computed by central differences, using a fine mesh (eight times the number of elements).

9.2.1. Sensitivity for a variable shape cavity

Figs. 9–11 show the value of the shape sensitivities of $u_x(A)$ and $t_x(B)$ with respect to the six shape parameters defined in Section 7.2. The continuous and discontinuous lines represent the modulus of the values computed numerically by the proposed procedure, while the dots are

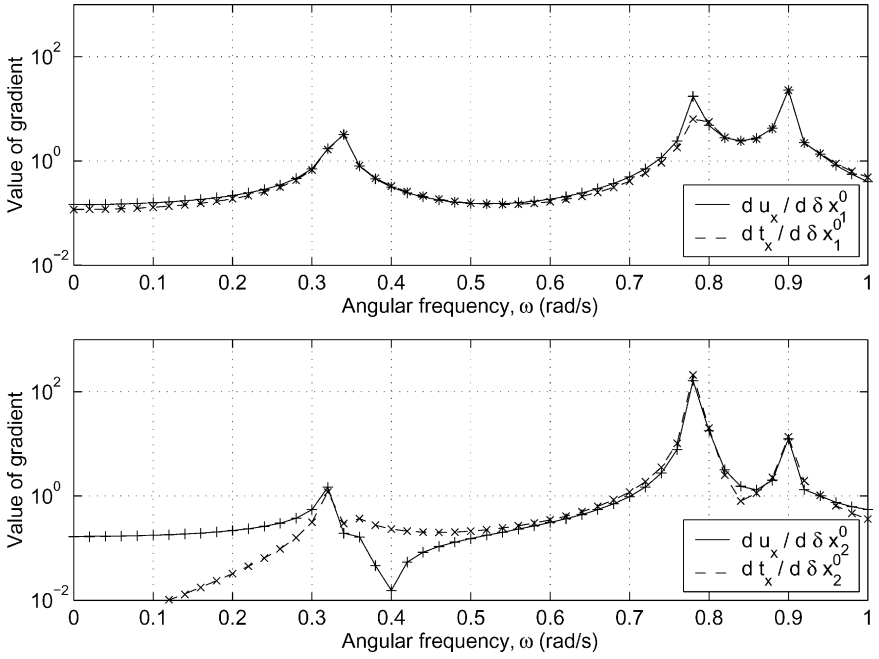

Fig. 13. Modulus of gradient for the variable elastic inclusion; continuous lines show the value obtained using δuBIE; dots, finite difference values. Upper graph, sensitivity with respect to, lower graph, sensitivity with respect to δx_2^0.

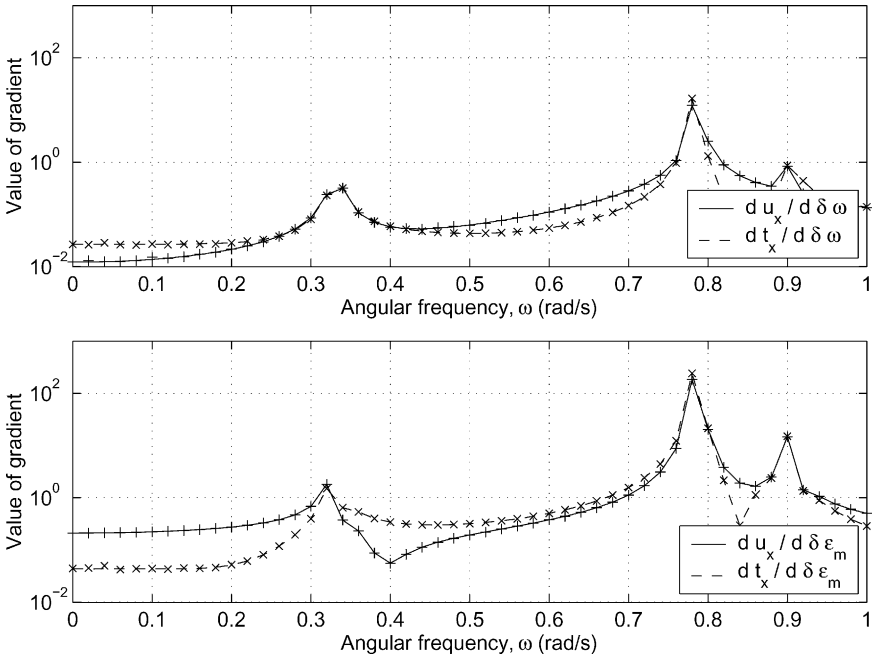

Fig. 14. Modulus of gradient for a variable ealastic inclusion; continuous lines show the value obtaine using δuBIE; dots, finite difference values. Upper graph, sensitivity with respect to $\delta\omega$, lower graph, sensitivity with respect to $\delta\varepsilon_m$.

the values computed by finite differences using a fine mesh (using $\times 8$ refinement). The results show an excellent agreement between the values computed with both procedures.

In Fig. 12 the ratio between the vertical displacement at point A and the applied stress is plotted, in order to show the dynamic behavior of the problem. Comparing this curve with the preceding ones, it is observed that the maxima of the sensitivity curves do not have any relationship with the natural frequencies of the plate. No deterioration close to or at eigen frequencies is observed. For all the parameters and both variables ($u_x(A)$, $q_x(B)$), the maximum is located at $\omega = 0.72$ rad/s, close to but lower than the third eigen frequency. This third eigen

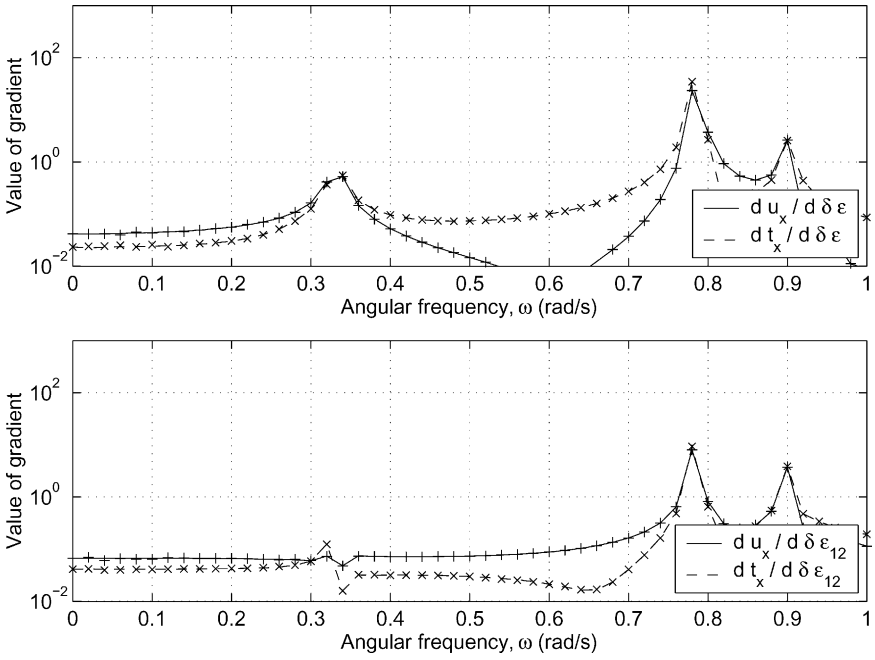

Fig. 15. Modulus of gradient for a variable elastic inclusion; continuous lines show the value obtained using δuBIE; does, finite difference values. Upper graph, sensitivity with respect to $\delta\varepsilon'$, lower graph, sensitivity with respect to $\delta\varepsilon_{12}$.

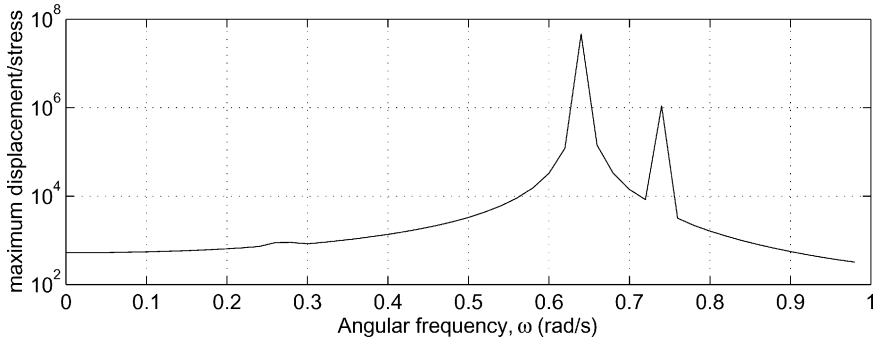

Fig. 16. Plate with a cavity: amplification factor for $u_y(A)$ vs. the excitation frequency.

frequency is actually due to the presence of the cavity, and therefore about this value the displacements and tractions are more sensitive to changes in its geometry. This is therefore a key consideration in the design of the defect identification experiments.

9.2.2. Sensitivity for a variable shape inclusion

Similar results are shown for the case of an elliptical inclusion. Figs. 13–16 show the value of the shape sensitivities of $u_x(A)$ and $t_x(B)$ with respect to the six shape parameters of the inclusion. Again, the lines represent the modulus of the values computed numerically by the proposed procedure, while the dots are the values computed by finite differences using a fine mesh. The results show an excellent agreement between the values computed with finite differences and direct differentiation, even close to the first two shown eigenfrequencies.

10. Conclusions

A shape sensitivity Integral Equation has been developed from the standard displacement Integral Equation through a linearization procedure. The equation has been carried to the boundary through a limiting process which leads to a shape Sensitivity Boundary Integral Equation. This equation includes a new free term which vanishes for the case of smooth boundary collocation points, but which appears to have been neglected previously. It is valid for harmonic dynamic elasticity in 2D, which is extensible to transient elastodynamics by a Fourier transform.

All these developments are performed prior to any consideration about the discretization of the variables or the geometry, and prior to the parametrization.

The parametrization of the flaws is reduced to a *virtual deformation field*, representing linearly the *variation of the geometry*, and not the geometry itself. This procedure can be applied for cavities or inclusions of any shape.

The continuity conditions required by all the kernels, the discretization and the proposed parametrization are presented, assuring the applicability. Besides, all the necessary tools for the numerical implementation have been developed and checked.

Some tests have been performed to asses the applicability of the formulation and the accuracy of the proposed numerical solution procedure. The numerical values match the analytical ones, as shown for a simple problem with known exact solution, and converge rapidly to the exact ones after increasing the number of elements.

For problems with more complex geometries, the results have been compared to those obtained by central finite differences, using a fine mesh, and the results again are indistiguishable.

The procedure allows the computation of sensitivities for arbitrarily shaped cavities, inclusions and outer domains, and harmonic dynamic excitation at a range of frequencies. The accurate and effective computation of shape gradients is solved with this procedure, and can be integrated with any gradient base minimization algorithm to solve a general identification inverse problem.

References

[1] Aithal R, Saigal S. Shape sensitivity in thermal problems using BEM. Engng Anal Bound Elem 1995;15:115–20.

[2] Bezerra LM, Saigal S. A boundary element formulation for the inverse elastostatics problem (iesp) of flaw detection. Int J Numer Meth Engng 1993;36:2189–202.

[3] Bonnet M. Shape identification using acoustic measurements: A numerical investigation using boundary integral equation and shape differentiation. In: Bui HD, Tanaka M, editors. Inverse Problem Engng Mech, 1992. p. 191–200.

[4] Bonnet M. Boundary integral equations and material differentiation applied to the formulation of obstacle inverse problems. Engng Anal Bound Elem 1995;15:121–36.

[5] Bonnet M. A general boundary-only formula for crack shape sensitivity of integral functionals. Comptes Rendus de l'Académie des Sciences 1999;327(12):1215–21.

[6] Brebbia CA, Domínguez J. Boundary elements, an introductory course. CMP. New York: McGraw Hill; 1992.

[7] Burczyński T, Kane JH, Balakrishna C. Shape design sensitivity analysis via material derivative-adjoint variable technique for 3-D and 2-D curved boundary elements. Int J Numer Meth Engng 1995;38: 2839–66.

[8] Gallego R, Suárez J. Numerical solution of the variation boundary integral equation for inverse problems. Int J Numer Meth Engng 1999; 49:501–18.
[9] Gallego R. Solution of inverse problems by boundary integral equations without residual minimization. Int J Solids Struct 1999; 37:5629–52.
[10] Kirsch G. The effect of circular holes on stress distributions in plates. V.D.I. 1898;42.
[11] Kubo S. Classification of inverse problems arising in field problems and their treatments. In: Bui HD, Tanaka M, editors. Inverse Problems Engng Mech, 1992. p. 51–60.
[12] Lee BY, Kwak BM. Shape optimization of two-dimensional thermoelastic structures using boundary integral equation formulation. Comput Struct 1991;41(4):709–22.
[13] Mellings SC, Aliabadi MH. Flaw identification using the boundary element method. Int J Numer Meth Engng 1995;38:399–419.
[14] Meric RA. Differential and integral sensitivity formulations and shape optimization by BEM. Engng Anal Bound Elem 1995;15: 181–8.
[15] Nishimura N, Kobayashi S. Determination of cracks having arbitrary shapes with the boundary integral equation method. Engng Anal Bound Elem 1994;15:189–95.
[16] Rus G, Gallego R. Solution of identification inverse problems by a sensitivity boundary integral equation. In: Suárez B, Oñate E, Bugeda G, editors. ECCOMAS2000.
[17] Goodier JN, Timoshenko S. Theory of elasticity. New York: McGraw-Hill; 1951.
[18] Tanaka M, Masuda Y. Boundary element method applied to some potential inverse problems. Engng Anal 1989;3–3:138–43.
[19] Yao Z, Gong B. Defect identification using boundary element methods of elastostatics. In: Tanaka, Bui et al, editors. Inverse problems in engineering mechanics.